



Asymptomatic Diagnosis of Huanglongbing Disease Using Metalloporphyrin Functionalized Single-Walled Carbon Nanotubes Sensor Arrays

Hui Wang^{1,2,3,5}, Pankaj Ramnani³, Tung Pham³, Claudia Chaves Villarreal⁴, Xuejun Yu³, Gang Liu^{1*} and Ashok Mulchandani^{3*}

OPEN ACCESS

Edited by:

Jiandong Pang,
Texas A&M University, United States

Reviewed by:

Yingmu Zhang,
University of Southern California,
United States
Suresh Kumar Kalangi,
Amity University Gurgaon, India

*Correspondence:

Ashok Mulchandani
adani@enr.ucr.edu
Gang Liu
pac@cau.edu.cn

Specialty section:

This article was submitted to
Nanoscience,
a section of the journal
Frontiers in Chemistry

Received: 05 December 2019

Accepted: 07 April 2020

Published: 12 May 2020

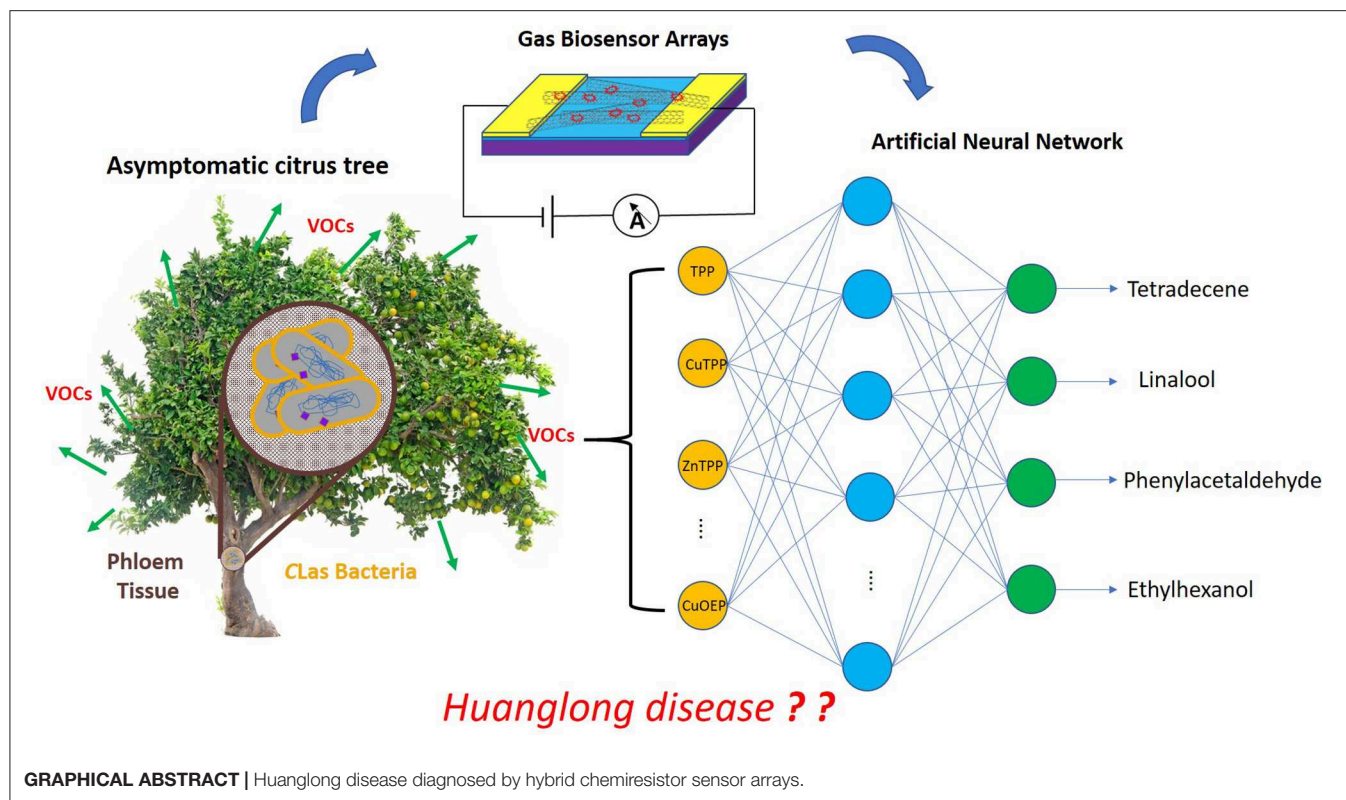
Citation:

Wang H, Ramnani P, Pham T, Villarreal CC, Yu X, Liu G and Mulchandani A (2020) Asymptomatic Diagnosis of Huanglongbing Disease Using Metalloporphyrin Functionalized Single-Walled Carbon Nanotubes Sensor Arrays. *Front. Chem.* 8:362. doi: 10.3389/fchem.2020.00362

¹ Key Laboratory of Modern Precision Agriculture System Integration Research, Ministry of Education and Key Laboratory of Agricultural Information Acquisition Technology, Ministry of Agriculture China Agricultural University, Beijing, China, ² State Key Laboratory of Animal Nutrition, Institute of Animal Science, Chinese Academy of Agricultural Sciences, Beijing, China, ³ Department of Chemical and Environmental Engineering and Materials Science and Engineering Program, University of California, Riverside, Riverside, CA, United States, ⁴ Escuela de Ciencia e Ingeniería de Materiales, Centro de Investigación y Extensión de Materiales, Instituto Tecnológico de Costa Rica, Cartago, Costa Rica, ⁵ Research Institute of Wood Industry, Chinese Academy of Forestry, Beijing, China

Porphyrins, with or without metal ions (MPs), have been explored and applied in optical and electrochemical sensor fields owing to their special physicochemical properties. The presence of four nitrogen atoms at the centers of porphyrins means that porphyrins chelate most metal ions, which changes the binding ability of MPs with gas molecules via non-specific binding. In this article, we report hybrid chemiresistor sensor arrays based on single-walled carbon nanotubes (SWNTs) non-covalently functionalized with six different MPs using the solvent casting technique. The characteristics of MP-SWNTs were investigated through various optical and electrochemical methods, including UV spectroscopy, Raman, atomic force microscopy, current-voltage (I-V), and field-effect transistor (FET) measurement. The proposed sensor arrays were employed to monitor the four VOCs (tetradecene, linalool, phenylacetaldehyde, and ethylhexanol) emitted by citrus trees infected with Huanglongbing (HLB), of which the contents changed dramatically at the asymptomatic stage. The sensitivity to VOCs could change significantly, exceeding the lower limits of the SWNT-based sensors. For qualitative and quantitative analysis of the four VOCs, the data collected by the sensor arrays were processed using different regression models including partial least squares (PLS) and an artificial neural network (ANN), which further offered a diagnostic basis for Huanglongbing disease at the asymptomatic stage.

Keywords: citrus greening disease, carbon nanotube, metalloporphyrin, chemiresistor, volatile organic compounds, artificial neural networks (ANN), gas sensor



INTRODUCTION

Porphyrins (Auwarter et al., 2015; Gutiérrez-Cerón et al., 2016), known as one of the critical types of biological ligands, are macromolecular heterocyclic compounds consisting of four modified pyrrole rings, which are connected together through a methine bridge so that the molecule takes the form of a large ring (Zahou et al., 2016). Each pyrrole ring is made from four carbons and one nitrogen. All of the nitrogen atoms located at the interior of the large ring form a central cavity that can coordinate with most metal ions to form metalloporphyrin complexes (MPs). Due to the coordinated metal ions of MPs being in an unsaturated state, MPs can bind with one or two additional ligands at the axial position. MPs can combine with gas molecules through Van der Waal forces, hydrogen bonding, or interaction with the central metal ion (Penza et al., 2010; Shirsat et al., 2012). The optical and electrical properties will change sharply when MPs interact with gas molecules. Therefore, sensors decorated with different MPs or MP hybrid materials are considered to be excellent gas-sensing devices at room temperature (Liu et al., 2010), of which the sensing performance has been investigated by several groups. Song and coworkers (Song et al., 2016) used 5, 10, 15, 20-tetrakis(4-aminophenyl)porphyrin zinc (ZnTAP) and nanoporous anodized aluminum oxide membrane to assemble highly ordered nanotubes of ZnTAP, which was applied to detect NO₂ at ambient temperature with high sensitivity and fast response-recovery time. Xie et al. developed a nitric oxide (NO) sensor based on a reduced graphene oxide field-effect transistor

functionalized with iron-porphyrin. This gas sensor for real-time monitoring of NO released from cultured human cells measured NO in living cells with high sensitivity and specificity (Xie et al., 2016).

Single-walled carbon nanotubes (SWNTs) (Peng et al., 2016), one-dimensional structures with a nanometer-range diameter, are seamless cylinders comprised of a layer of graphene. They have gained widespread use in electrochemical sensors due to their interesting properties, such as excellent electrical conductivity, high surface-to-volume ratio, and thermostability (Salvetat et al., 1999; Kang et al., 2007). Studies indicate that gas molecules as either charge donor or a charge acceptor can be weakly adsorbed by SWNTs, which can cause a significant change in the electronic transport properties of SWNTs in view of charge transfer and charge fluctuation (Britz and Khlobystov, 2006; Giraldo et al., 2014). However, the low sensitivity and poor selectivity of bare SWNT-based sensors limit the ability of an individual sensor to analyze a multi-component gas mixture. Surface modifications that occur when SWNTs are functionalized with gas-sensitive materials can enhance sensing performance (Martin et al., 2013; Hijazi et al., 2014). MPs have flat and planar structures that efficiently bind with the SWNTs through π - π interactions (Bassiouk et al., 2013).

Huanglongbing (HLB), also called citrus greening or yellow shoot disease, is a bacterial disease of citrus caused by a vector-transmitted pathogen (Sagaram et al., 2009) that threatens the multi-billion dollar citrus industry all over the world (Bassanezi et al., 2011). There are two general means of propagation:

(i) transmission from infected citrus trees to the surrounding trees by citrus psyllid insects (Grafton-Cardwell et al., 2013); (ii) grafting of an infected scion on a healthy citrus tree. In reality, if a citrus tree is infected by HLB, the disease will incubate for several years without any symptoms (Lee et al., 2015) and then exhibit visible symptoms, including yellowing of the veins, splotchy mottling of the entire leaf, dieback of twigs, and decay of feeder rootlets and lateral roots (Johnson et al., 2014). There are few effective and cheap treatments to cure this disease. The most frequently used method is to remove infected trees selectively, halting the spread of HLB, wherefore early detection of this disease is vital. In 2020, an approach to eradicate the bacteria responsible for Huanglongbing disease using silver nanoparticles (AgNPs) achieved remarkable results, providing a new method to cure this disease (Stephano-Hornedo et al., 2020). However, it is especially challenging to diagnose HLB at an early stage due to the infected trees lacking symptoms while still acting as reservoirs to transmit the disease. Current detection methods for HLB are based on qualitative assessment of disease symptoms and molecular analysis methods such as visible-near infrared spectroscopy (Sankaran et al., 2011), mid-infrared (MIR) spectroscopy (Sankaran et al., 2010), enzyme-linked immunosorbent assay (ELISA) (Rapala et al., 2002), and polymerase chain reaction (PCR) (Ananthakrishnan et al., 2010). These techniques are susceptible to error and require expensive, time-consuming processes, which makes them unsuitable for rapid, on-site detection at the asymptomatic stage. Previous research has demonstrated that the VOCs released by the trees are closely associated with plant metabolism, which offers a new means for detecting the status of plant health at any stage. Aksenov et al. (2014) used gas chromatography/differential mobility spectrometry (GC/DMS) to analyze the VOCs released by the Huanglongbing infected citrus tree. Hundreds of independent VOC measurements were collected and analyzed through GC/DMS. Based on changes in the concentrations of characteristic VOCs, the infection process was divided into four stages: healthy, asymptomatic, mild, and severe. They found that the contents of VOCs (tetradecene, linalool, nonadecane, phenylacetaldehyde, and ethylhexanol) changed dramatically at the asymptomatic stage. The levels of tetradecene and ethylhexanol decreased, and the rest increased. They established VOC-based disease detection with high accuracy. But GC/DMS is an expensive device that requires professional operation. To overcome this limitation, this paper proposes an electronic gas sensor to replace GC/DMS so as to determine the VOC concentrations at high sensitivity and low cost.

Here, hybrid chemiresistive sensor arrays based on SWNTs non-covalently functionalized with MPs was fabricated that is easy to use and low-cost and which is suitable for the detection of VOCs released from Huanglongbing infected citrus trees at the asymptomatic stage. The characteristics of MP-SWNTs were measured by optical and electrical methods, including UV-vis absorption spectroscopy, Raman, atomic force microscopy, current-voltage (I-V), and field-effect transistor (FET) measurement. The sensor arrays were applied to monitor the concentrations of the VOCs tetradecene, linalool, phenylacetaldehyde, and ethylhexanol. To discriminate the four VOCs qualitatively and quantitatively, partial least squares (PLS)

and an artificial neural network (ANN) were further selected to process the data recorded by the sensor arrays.

MATERIALS AND METHODS

Chemicals and Materials

Dispersed single-walled carbon nanotube solution (0.01 mg/ml, 95% semiconducting) was obtained from Nano-Integris Inc. (USA). Chemical reagents (dimethylformamide, acetone, propanol, and ammonium hydroxide) were purchased from Fisher Scientific Company (USA). Three volatile organic compounds (2-Ethyl-1-hexanol, 1-tetradecene, and phenylacetaldehyde) and 3-aminopropyltriethoxysilane (APTES) were purchased from Sigma Aldrich (USA). The MPs, namely tetraphenyl porphyrin (TPP), iron porphyrin (FeTPP), copper porphyrin (CuTPP), zinc porphyrin (ZnTPP), copper octamethyl porphyrin (CuOEP), and manganese OEP (MnOEP), were provided by two chemical companies, Sigma-Aldrich (USA) and Frontier Scientific (USA). Deionized water was used throughout the experiments.

The dispersed solutions of MPs (TPP, FeTPP, ZnTPP, and MnOEP) were prepared by dissolving a certain weight into 10 ml N, N-dimethylformamide (DMF) under ultrasonication. Saturated solutions of CuTPP and CuOEP were prepared for further use.

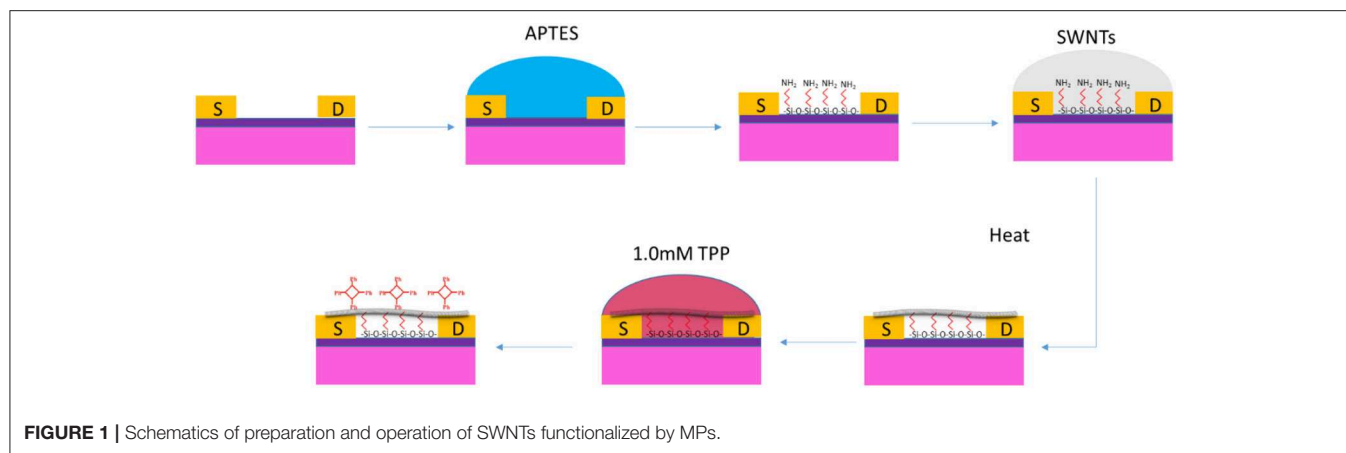
Apparatus

The spectral, morphological, and electrical characteristics of SWNTs before and after being functionalized by MPs were investigated by atomic force microscopy (AFM), Raman, UV-Vis spectrometry, current-voltage (I-V), and field-effect transistor (FET) measurement. AFM images were obtained using an atomic force microscope (Veeco Innova, Santa Barbara, CA, USA). Raman spectra were measured with a Nicolet Omega XR Dispersive microscope with 532-nm laser excitation. The UV spectrum was acquired by a Beckman DU640 UV/Vis spectrophotometer (Beckman Coulter, Inc. USA). Electrical measurements were made using a semiconductor parameter analyzer (Keithley 2636, USA).

For FET measurements, the Si substrate was covered with gold film, which served as the base, and charged with a linear voltage ranging from -60 V to $+20$ V. The two gold electrodes etched on the SiO₂ surface acted as the drain and source, to which a constant voltage (0.1 V) was applied. A dielectric layer of 100-nm thick SiO₂ was used to separate the base from the source-drain.

Fabrication of MPs-SWNTs

The sensor was designed with a single-gap structure because this offers a large area over which to react with gas molecules, and electrical conductivity can be controlled easily in comparison with an interdigital electrode. Highly p-doped silicon with a 100-nm SiO₂ layer was employed to fabricate the single gap microelectrode (10 μ m in width and 10 μ m in length) by photolithography using the positive photoresist AZ-5214. A 20-nm Cr layer and a 180-nm Au layer were uniformly deposited and etched on the surface of the Si/SiO₂ via e-beam evaporation. Finally, the photoresist residual was cleaned away with acetone solution.



The modification was shown in **Figure 1**. The single-gap electrode was flushed successively with acetone and isopropanol and then blow-dried in streaming air to remove surface impurities before use. The electrode was immersed into ammonium hydroxide for 30 min, and the residue was rinsed off with sufficient deionized water. The cleaned electrode was incubated in 0.5 mL APTES for 60 min, washed with deionized water, and blow-dried using a nitrogen stream as quickly as possible. After that, a 5- μ L SWNT solution was added to cover the microelectrode, and it was incubated with a high-humidity and dark condition for 60 min. The residual SWNTs were then carefully cleaned away with deionized water, and the electrode was annealed in ambient air at 250°C for 60 min. For MP immobilization, the single-gap electrode decorated with SWNTs (SWNTs-FET) was immersed in different MPs and placed in the dark for 4 h. Finally, the MP-SWNTs was annealed at 90°C under inert gasses in a protected condition for 60 min.

Gas Sensing Setup

The gas sensing setup shown in **Figure S1** was designed and integrated to perform VOC determination. This device can generate different concentrations of VOCs by mixing different proportions of air and saturated vapors of VOCs, which flowed through a 1.2 cm³ sealed glass dome covering the sensor array. A Keithley 2636 was used as a data-collecting device, connecting to the sensor arrays via three meters (bias, drain, and source) and recording output voltage and input current. All devices were controlled by the software installed in the computer that was programmed with the Laboratory Virtual Instrument Engineering Workbench (Lab VIEW). For experimental measurement, a voltage of +0.1 V was applied between the drain and the source without the base voltage. Before detecting a desired concentration of VOC, the sensor array was exposed to dry air until it reached a stable baseline.

RESULTS AND DISCUSSION

Characteristics of MP-SWNTs

Electrical characteristics (I_{DS} - V_{DS} and I_{DS} - V_G), AFM, UV spectrometry, and Raman were used to investigate the

characteristics of SWNTs before and after functionalization with MPs.

Electrical characterization is an effective method for distinguishing the changes in conductivity or resistance of SWNTs before and after each modification. As shown in **Figure 2A**, the I_{DS} - V_{DS} curves of bare SWNTs and CuTPP-SWNTs presented good linear relationships, but the current decreased dramatically with CuTPP-SWNTs. As shown in **Figure S2**, the resistance values of bare SWNTs and CuTPP-SWNTs were 28 and 318 k Ω , respectively; thus, with the addition of CuTPP, the resistance increased 11 times in comparison with bare SWNTs. The poor conductivity of CuTPP-SWNTs illustrated that the molecules of CuTPP had interacted with the carbon nanotube sidewalls, forming specific π - π -interactions through non-covalent interactions (Li et al., 2004; Shirakawa et al., 2005). The change in conductivity may be attributed to a couple of different causes (Zhao and Stoddart, 2009): (i) the carrier concentration (n) may be changed by an electron/charge-transfer between CuTPP and SWNTs; (ii) CuTPP may act as a randomly distributed scattering potential, transforming the mobility (μ) of the charge carrier. The FET curves of bare SWNTs before and after functionalization with CuTPP are shown in **Figure 2B**, for which the two electrodes were exposed to the air. We found that the threshold gate voltage (V_{TH}) of bare SWNTs was about -13.5 V, while when the SWNTs were functionalized with CuTPP, the FET curves shifted in the negative direction and the V_{TH} value was -20 V. According to the mobility equation, the mobility values of bare SWNT and CuTPP-SWNTs are 176 and 136 cm²/Vs, respectively, which is in agreement with the I_{DS} - V_{DS} results. The results remarkably demonstrate that the positive hole of the p-type semiconductor SWNTs was occupied by the electron, resulting in a lower barrier concentration and carrier mobility.

The morphology of bare SWNTs and CuTPP-SWNTs was studied by AFM observation in **Figure 3**. It was clear that the height of bare SWNTs was about 1.7 nm, approximately equal to the theoretical value (Bandow et al., 1998), which also matched the diameter value for the SWNTs offered by the producer. The height of the CuTPP-functionalized SWNTs was noticeably increased to 4 nm as a consequence of the attachment of porphyrin to the SWNTs' surface.

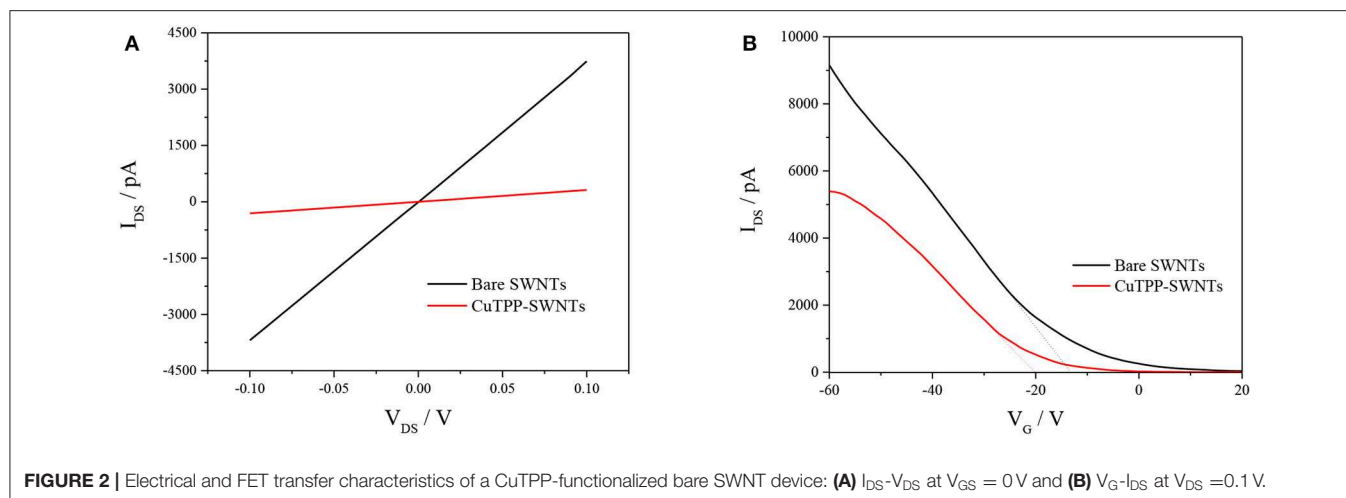


FIGURE 2 | Electrical and FET transfer characteristics of a CuTPP-functionalized bare SWNT device: **(A)** I_{DS} - V_{DS} at $V_{GS} = 0$ V and **(B)** V_G - I_{DS} at $V_{DS} = 0.1$ V.

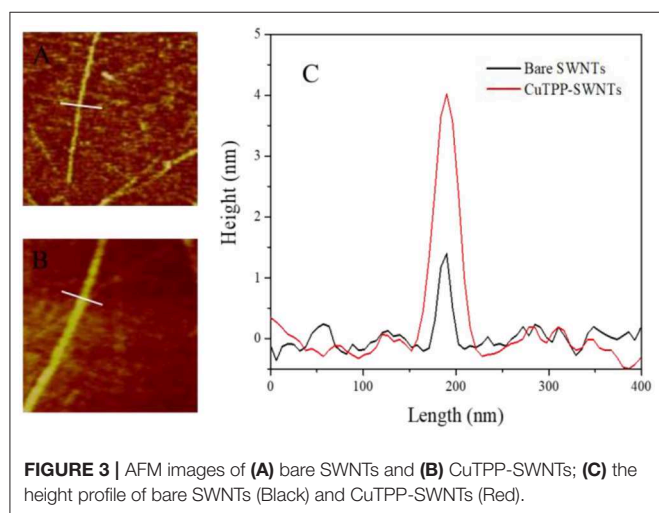


FIGURE 3 | AFM images of **(A)** bare SWNTs and **(B)** CuTPP-SWNTs; **(C)** the height profile of bare SWNTs (Black) and CuTPP-SWNTs (Red).

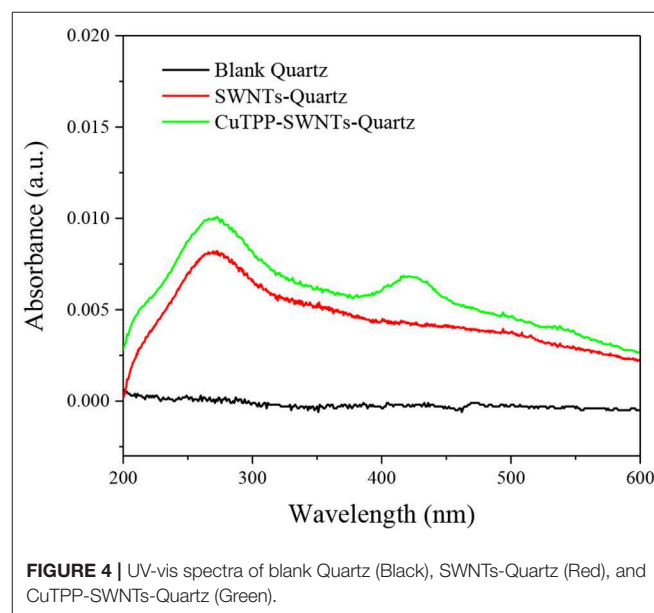


FIGURE 4 | UV-vis spectra of blank Quartz (Black), SWNTs-Quartz (Red), and CuTPP-SWNTs-Quartz (Green).

The formation of CuTPP-SWNTs is further confirmed by UV absorbance because most MPs have a strong near-UV band [a sharp, intense Soret band (B band)] in the near UV region and two weak Q bands responsible for the red to purple color in the visible region. Here, we chose a quartz plate to replace the silicon substrate due to its good optical transparency. Compared to blank Quartz in **Figure 4**, SWNTs-Quartz had an absorption peak at 273 nm and an increasing absorbance intensity in the whole spectral range, suggesting that the opaque material of SWNTs had attached to the Quartz (Ryabenko et al., 2004). The network structure formed by this attachment hampers parts of light from moving through it. After SWNTs were functionalized with CuTPP, a transmitting B band at 418 nm and one Q band at 541 nm were observed, which demonstrate that CuTPP was covalently attached to the surface of the SWNTs (Mammana et al., 2008; Wang et al., 2011).

The interactions between the SWNTs and CuTPP were characterized using Raman spectroscopy, and the results are shown in **Figure 5**. The Raman spectrum of SWNTs shows four

peaks at $1,351\text{ cm}^{-1}$ (a small D band), $1,579\text{ cm}^{-1}$ (a G^- band), $1,600\text{ cm}^{-1}$ (a sharp G^+ band), and $2,680\text{ cm}^{-1}$ (2D band). After CuTPP was non-covalently linked to SWNTs, the G^+ band peak becomes narrower, and the G^+ band shifts to $1,598\text{ cm}^{-1}$, suggesting that it can be ascribed to electron doping between SWNTs and CuTPP. Meanwhile, the D/G intensity ratio of CuTPP-SWNTs increase in comparison with SWNTs, indicating the conversion of sp^2 carbons to sp^3 carbons on the SWNTs surfaces due to the functionalization (Geng and Jung, 2010).

Gas Sensing Performance

As discussed earlier, the VOCs can serve as biomarkers to diagnose whether a citrus tree is infected by HLB. To evaluate the sensing performance of MP-functionalized SWNTs devices, we measured the real-time electrical response of the hybrid chemiresistor sensor arrays to phenylacetaldehyde, tetradecene,

linalool, and ethylhexanol vapors with concentrations varying from 5 to 100% of saturated vapors at room temperature. A normalization method was adopted to process the electrical signal, reducing the differences caused by the modification. The normalized response is defined as a relative change in resistance:

$$\Delta R/R_0 \% = (R - R_0)/R_0 \times 100\% \quad (1)$$

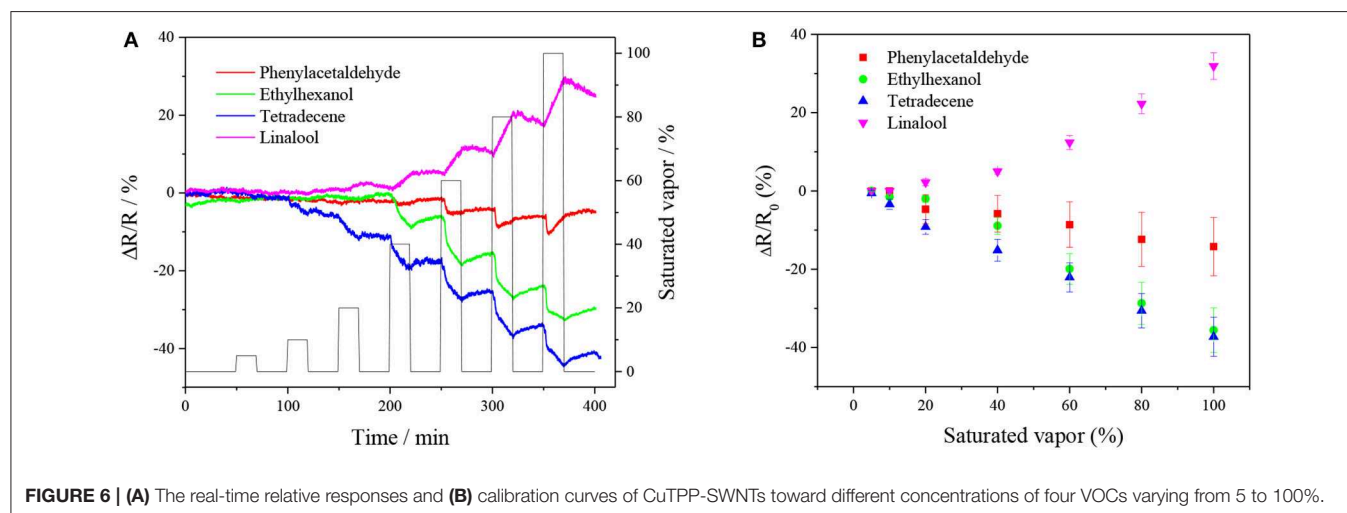
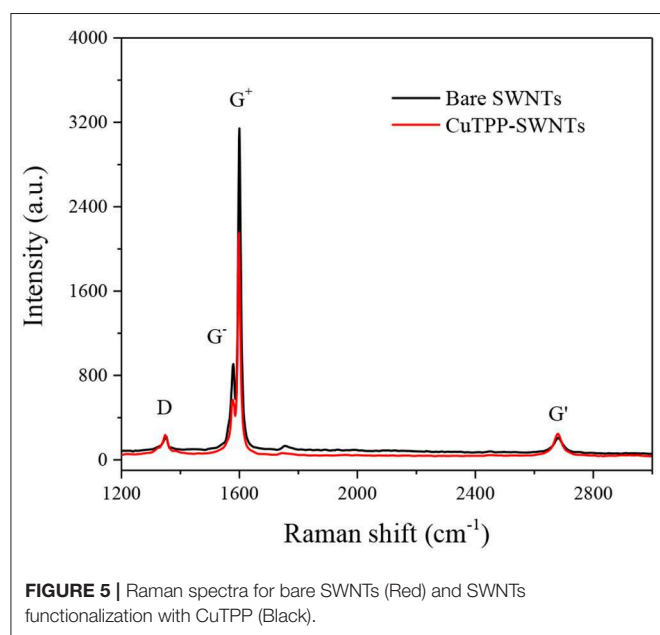
where R_0 is the value of initial baseline resistance before MP-SWNTs are exposed to VOCs and R is the value of resistance after MP-SWNTs are exposed to VOCs.

Figure 6A shows the normalized resistance of CuTPP-SWNTs toward the four VOCs (tetradecene, linalool, phenylacetaldehyde, and ethylhexanol) released by infected citrus trees at the asymptomatic stage. The normalized resistance

of CuTPP-SWNTs displayed a correlation with the VOC concentrations in the **Figure 6B**. The conductivity of CuTPP-SWNTs was increased after CuTPP-SWNTs had been exposed to tetradecene, ethylhexanol, and phenylacetaldehyde, while, in CuTPP-SWNTs exposed to linalool, the conductivity decreased. The reason for this is discussed in Mechanism section. Compared with the sensing responses of bare SWNTs shown in **Figure S3**, the sensitivity of CuTPP-SWNTs to the VOCs (except for phenylacetaldehyde) was improved to different degrees. For 100% saturated tetradecene vapor, the normalized response of bare SWNT is only 0.83%, with the response reaching 50% of the maximum in 4 min, as shown in **Figure S4**. However, the normalized response of CuTPP-SWNTs was 45 times higher than that of bare SWNTs at the same concentration, and 50% of the maximum response was reached in <5 min. Similar fast responses were observed using the rest of the MP functionalized SWNT devices to test the four VOCs; the related data are shown in **Tables S1–S4**. This indicates that the modification of SWNTs with MPs can enhance sensitivity, selectivity, and response time in detecting gas concentration. As shown in **Table S5**, the lowest detection limits were 4.86, 10.15, 0.18, and 0.61 ppm for phenylacetaldehyde, ethylhexanol, tetradecene, and linalool, respectively. After each experiment, we found that the sensor arrays needed a long time to recover to the baseline, but it was possible to shorten the recovery time by exposing the sensor arrays to UV light or a high-temperature environment in an oven, which can enhance the rate of desorption.

Mechanism

The sensing mechanism for the field-effect transistor includes four aspects: electrostatic gating, changes in gate coupling, Schottky barrier effects, and carrier mobility changes (Heller et al., 2008). CuTPP-SWNTs were selected to investigate the sensing mechanism upon interaction with organic gas molecules. Prior to FET detection, CuTPP-SWNTs were exposed to steaming air or saturated VOC vapors for 60 min to ensure that the gas molecules could interact adequately with the gas-sensitive material of CuTPP-SWNTs. **Figure 7** shows the transfer



characteristics (I_{DS} - V_G) curves. Compared to the FET curve in dry air, the I_{DS} - V_G curves of phenylacetaldehyde shifted in the negative direction, and the threshold gate voltage (V_{TH}) was

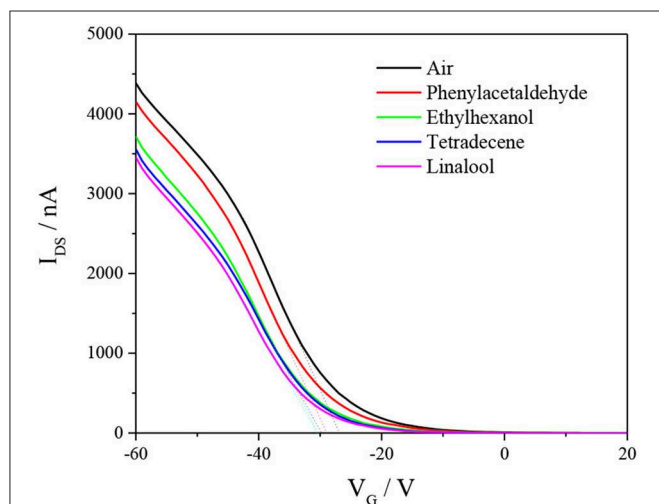


FIGURE 7 | Transfer characteristics (I_{DS} - V_G curves at $V_{DS} = -0.1$ V) of CuTPP-SWNTs in the presence of air and different saturated VOCs.

decreased, which was mainly ascribed to the electrostatic gating effect. According to the mobility equation, the values of carrier mobility of ethyl hexanol, tetradecane, and linalool reduced compared to the mobility for dry air. Thus, a threshold voltage shift and change in carrier mobility in the case of exposure of the CuTPP-SWNT hybrid to ethyl hexanol, tetradecane, and linalool indicate that the sensing mechanism is mainly governed by electrostatic gating and carrier mobility changes in combination.

Mathematical Model for VOC Analysis

Pattern recognition tools can provide powerful multivariate analysis methods to extract specific non-related information from complex correlations and have been widely applied in the multisensory field. Herein, we chose linear and non-linear models to process the data collected by the hybrid chemiresistor sensor arrays for the qualitative and quantitative analysis of the four VOCs. Principal component analysis (PCA) was performed, and the results are shown in **Figure S5** and **Table S6**.

Partial Least Square Regression (PLSR)

PLSR (Mehmood et al., 2012), a multivariate calibration model, was used to deal with the two multivariable matrices (X_0 and Y_0) with significantly redundant variations. It is realized by extracting predictor variables (X and Y) from the block X_0 -matrix and

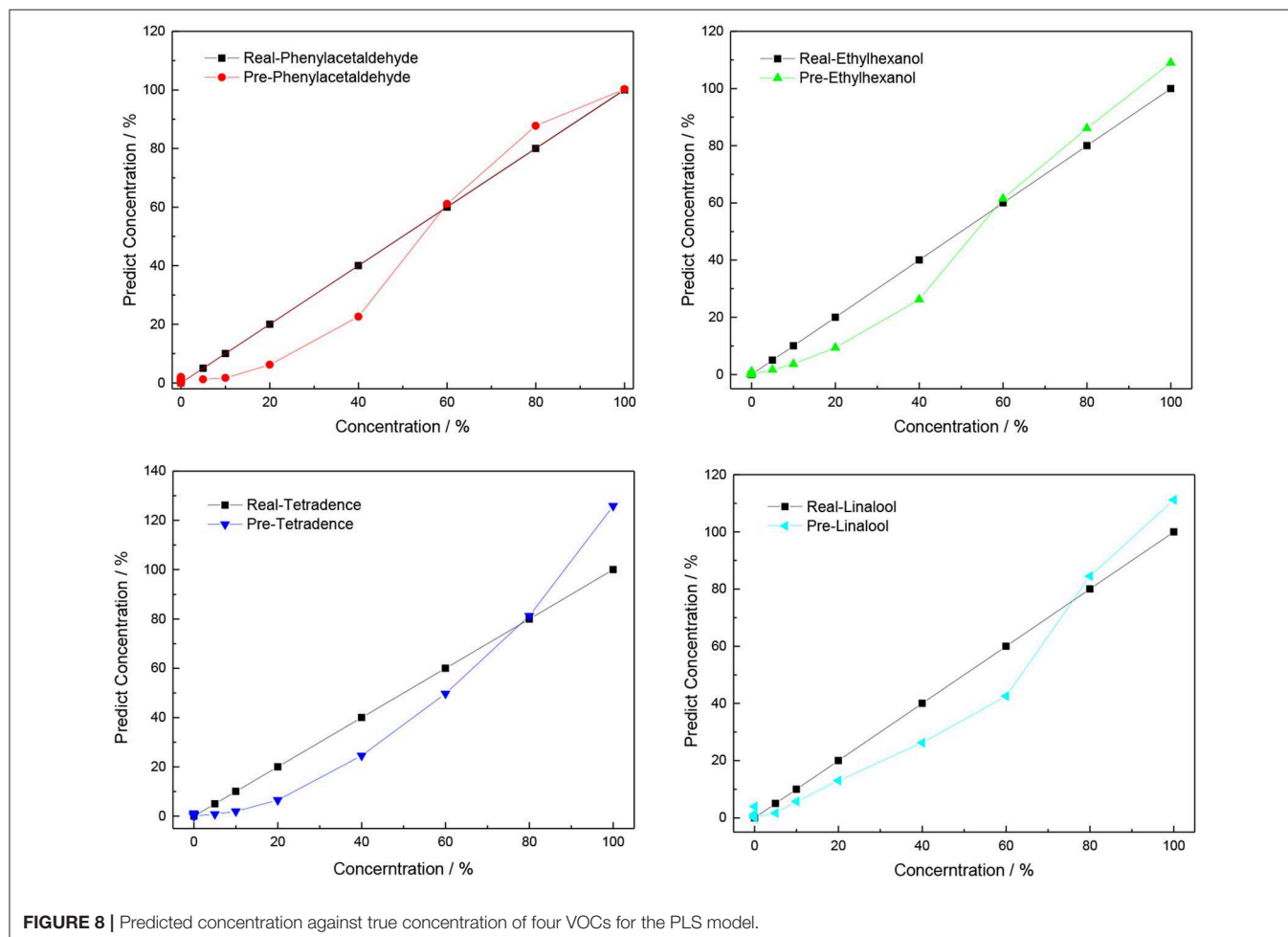
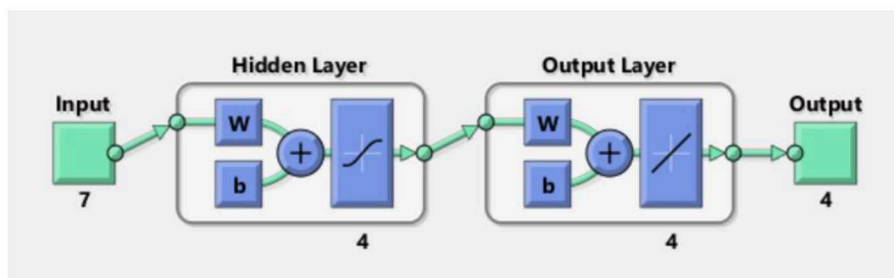
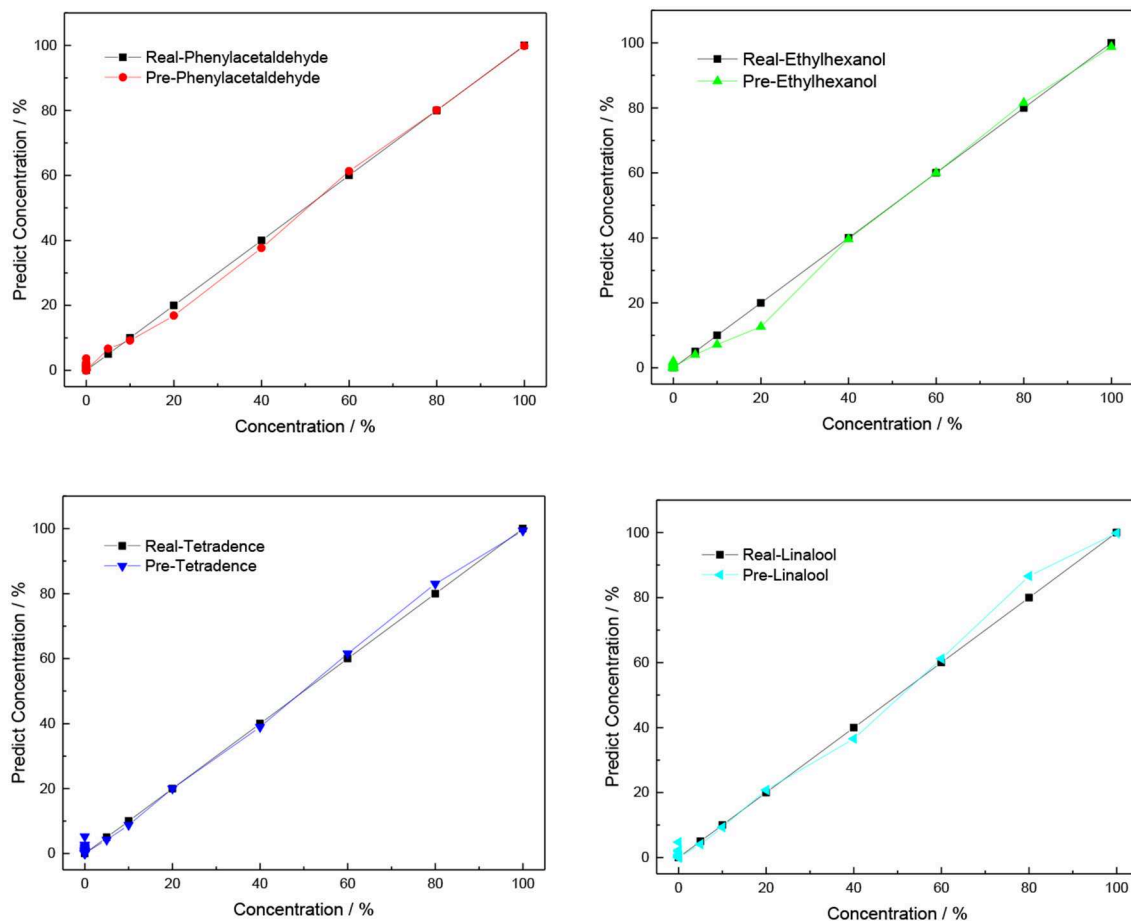


FIGURE 8 | Predicted concentration against true concentration of four VOCs for the PLS model.

TABLE 1 | The correlation coefficient (R_0) and root mean square error (R_{SMT}) between real concentrations and predicted concentrations.

	Phenylacetaldehyde		Ethylhexanol		Tetradecene		Linalool	
	R_0	R_{SMT}	R_0	R_{SMT}	R_0	R_{SMT}	R_0	R_{SMT}
PLSR	0.92816	9.58762	0.98718	4.11176	0.98303	4.72537	0.9762	5.58669
SPLS	0.98321	4.82493	0.98924	4.12993	0.9734	6.75741	0.98067	5.14909
ANN	0.99883	1.33108	0.99784	1.69709	0.99861	1.53506	0.99794	1.80906

**FIGURE 9** | Type of architecture of the neural network.**FIGURE 10** | Predicted concentration against true concentration of four VOCs for the ANN model.

the block Y_0 -matrix and then analyzing and establishing the relationship between the block X -matrix and the block Y -matrix. PLSR combines the merits of principal component analysis and multiple linear regression. This analysis also suits small samples with a simplified data structure.

For this experiment, the X_0 -matrix consists of 28 columns and 7 rows, with different concentrations (corresponding to 5, 10, 20, 40, 60, 80, and 100% saturated vapors) of four VOCs as the columns and normalized responses of MP-functionalized SWNTs (bare SWNTs, TPP-SWNTs, CuTPP-SWNTs, FeTPP-SWNTs, ZnTPP-SWNTs, CuOEP-SWNTs, MnOEP-SWNTs) as rows, and the Y_0 -matrix consists of 28 columns and 4 rows by using the real concentration as the columns and the four VOCs as the rows. As the normalized responses (X_0 -matrix) are non-linear with the concentrations of VOCs (Y_0 -matrix), these data matrices need to be pre-processed prior to use: $X = X_0$, $Y = \text{Sqrt}(Y_0)$. After the pre-treatment, the relationship between X and Y approximates linearity. The X -matrix and Y -matrix are inputted into the PLSR model, and the result is shown in **Figure S6** and **Figure 8**. We found that the correlation coefficient between the real concentration and fit concentration was much higher and the standard deviation was lower than the matrix without pretreatment; the data are presented.

Artificial Neural Network

An artificial neural network (ANN) (Asilturk and Cunkas, 2011) is a flexible mathematical structure that is capable of identifying complex non-linear relationships between input and output data sets. ANN models have been found to be useful and efficient, particularly in problems for which the characteristics of the processes are difficult to describe using physical equations. The overall structure is shown in **Figure 9**. The procedures of ANN are divided into three main parts: an input layer, hidden layers, and an output layer. In this model, the X matrix is the input layer, which consists of 28 columns and 7 rows filled by using different concentrations (corresponding to 5, 10, 20, 40, 60, 80, and 100% saturated vapors) of four VOCs as the columns and normalized responses of MP-functionalized SWNTs (bare SWNTs, TPP-SWNTs, CuTPP-SWNTs, FeTPP-SWNTs, ZnTPP-SWNTs, CuOEP-SWNTs, and MnOEP-SWNTs) as rows. The Y matrix is selected as an output layer, which consists of 4 columns and 28 rows, with the four concentrations in each row corresponding to each column of X . The data of the X matrix are divided randomly into three sets: 60% as training samples, 10% as validation samples, and 30% as testing samples. During learning, output values from the ANN are compared to true values, and the coupling weights are adjusted to give a minimum sum of square errors. After testing and comparing, we found that four nodes of the hidden layer can cause the average relative error to reach a minimum, shown in **Figure S7** and **Figure 10**.

Among the three mathematical models, PCA is used only for qualitative analysis of VOCs emitted by infected citrus trees, and it is hard to acquire accurate results when the gas concentration of any VOC is below 20%. Both PLSR and ANN are simple methods that can offer qualitative and quantitative information, which is widely employed in stoichiometry. The correlation coefficient (R_0) and root mean square error (R_{SMT}) between

real concentrations and predicted concentrations are shown in **Table 1**. We found that the best result is achieved with the utilization of the ANN model because the values of R_0 for these VOCs are higher and the R_{SMT} is lower than with PLS and SPLS. This demonstrates that a non-linear regression model is well-suited for non-linear data processing.

CONCLUSIONS

Volatile organic compounds (VOCs; phenylacetaldehyde, tetradecene, linalool, and ethylhexanol) released by infected citrus trees are associated with plant metabolism and can serve as biomarkers for the detection of Huanglongbing disease (HLB). In conclusion, we have fabricated hybrid chemiresistor sensor arrays based on SWNTs functionalized with different MPs to determine changes in the concentrations of four VOCs emitted by infected citrus trees, which are used to diagnose HLB at an asymptomatic stage. Optical and electrochemical approaches have been applied to examine the electrical characterization of SWNTs before and after functionalization with MPs and have shown that MPs can attach to SWNTs to form a stable membrane. MP-SWNTs improved the sensitivity to the various VOCs tested, and are shown to have differences in sensing performance. To obtain accurate concentrations, the test data collected by the hybrid chemiresistor sensor arrays were analyzed using the PCA, PLSR, and ANN techniques. By comparing these three results, it was found that ANN was much better suited to the non-linear data processing required.

DATA AVAILABILITY STATEMENT

The raw data supporting the conclusions of this article will be made available by the authors, without undue reservation, to any qualified researcher.

AUTHOR CONTRIBUTIONS

HW: data curation, formal analysis, methodology, software, writing—original draft, reviewing, and editing. PR, TP, CV, and XY: formal analysis and methodology. GL: supervision, reviewing, and editing. AM: conceptualization, funding, resources, supervision, methodology, reviewing, and editing.

FUNDING

This work was supported by grants from the United States Department of Agriculture (No. 2014-67021-21589) to AM, the Chinese National Natural Science Foundation (No. 31671578), and Key Realm R&D Program of Guangdong Province (Nos. 2019B020215002 and 2019B020215004). AM acknowledges the financial support of W. Ruel Johnson Chair.

SUPPLEMENTARY MATERIAL

The Supplementary Material for this article can be found online at: <https://www.frontiersin.org/articles/10.3389/fchem.2020.00362/full#supplementary-material>

REFERENCES

- Aksenov, A. A., Pasamontes, A., Peirano, D. J., Zhao, W., Dandekar, A. M., Fiehn, O., et al. (2014). Detection of Huanglongbing disease using differential mobility spectrometry. *Anal. Chem.* 86, 2481–2488. doi: 10.1021/ac403469y
- Ananthkrishnan, G., Venkataprasanna, T., Roy, A., and Brlansky, R. N. (2010). Characterization of the mixture of genotypes of a Citrus tristeza virus isolate by reverse transcription-quantitative real-time PCR. *J. Virol. Methods* 164, 75–82. doi: 10.1016/j.jviromet.2009.12.001
- Asilturk, I., and Cunkas, M. (2011). Modeling and prediction of surface roughness in turning operations using artificial neural network and multiple regression method. *Expert Syst. Appl.* 38, 5826–5832. doi: 10.1016/j.eswa.2010.11.041
- Auwarter, W., Eciija, D., Klappenberger, F., and Barth, J. V. (2015). Porphyrins at interfaces. *Nat. Chem.* 7, 105–120. doi: 10.1038/nchem.2159
- Bandow, S., Asaka, S., Saito, Y., Rao, A. M., Grigorian, L., Richter, E., et al. (1998). Effect of the growth temperature on the diameter distribution and chirality of single-wall carbon nanotubes. *Phys. Rev. Lett.* 80, 3779–3782. doi: 10.1103/PhysRevLett.80.3779
- Bassanezi, R. B., Montesino, L. H. M., Gasparoto, C. G., Bergamin, A., and Amorim, L. (2011). Yield loss caused by huanglongbing in different sweet orange cultivars in so Paulo, Brazil. *Eur J Plant Pathol.* 130, 577–586. doi: 10.1007/s10658-011-9779-1
- Bassiouk, M., Basiuk, V. A., Basiuk, E. V., Álvarez-Zauco, E., Martínez-Herrera, M., Rojas-Aguilar, A., et al. (2013). Noncovalent functionalization of single-walled carbon nanotubes with porphyrins. *Appl. Surf. Sci.* 275, 168–177. doi: 10.1016/j.apsusc.2012.12.167
- Britz, D. A., and Khlbystov, A. N. (2006). Noncovalent interactions of molecules with single walled carbon nanotubes. *Chem. Soc. Rev.* 35, 637–659. doi: 10.1039/b507451g
- Geng, J. X., and Jung, H. (2010). Porphyrin functionalized graphene sheets in aqueous suspensions: from the preparation of graphene sheets to highly conductive graphene films. *J Phys Chem C* 114, 8227–8234. doi: 10.1021/jp1008779
- Giraldo, J. P., Landry, M. P., Faltermeier, S. M., McNicholas, T. P., Iverson, N. M., Boghossian, A. A., et al. (2014). Plant nanobionics approach to augment photosynthesis and biochemical sensing. *Nat. Mater.* 13, 400–408. doi: 10.1038/nmat3890
- Grafton-Cardwell, E. E., Stelinski, L. L., and Stansly, P. A. (2013). Biology and management of asian citrus psyllid, vector of the huanglongbing pathogens. *Annu. Rev. Entomol.* 58, 413–432. doi: 10.1146/annurev-ento-120811-153542
- Gutiérrez-Cerón, C., Páez, M. A., and Zagal, J. H. (2016). Reactivity descriptors for iron porphyrins and iron phthalocyanines as catalysts for the electrooxidation of reduced glutathione. *J Solid State Electrochem.* 20, 3199–3208. doi: 10.1007/s10008-016-3396-z
- Heller, I., Janssens, A. M., Mannik, J., Minot, E. D., Lemay, S. G., and Dekker, C. (2008). Identifying the mechanism of biosensing with carbon nanotube transistors. *Nano Lett.* 8, 591–595. doi: 10.1021/nl072996i
- Hijazi, I., Bourgeteau, T., Cornut, R., Morozan, A., Filoramo, A., Leroy, J., et al. (2014). Carbon nanotube-templated synthesis of covalent porphyrin network for oxygen reduction reaction. *J. Am. Chem. Soc.* 136, 6348–6354. doi: 10.1021/ja500984k
- Johnson, E. G., Wu, J., Bright, D. B., and Graham, J. H. (2014). Association of *Candidatus Liberibacter Asiaticus* root infection, but not phloem plugging with root loss on huanglongbing- affected trees prior to appearance of foliar symptoms. *Plant Pathol.* 63, 290–298. doi: 10.1111/ppa.12109
- Kang, S., Pinault, M., Pfefferle, L. D., and Elimelech, M. (2007). Single-walled carbon nanotubes exhibit strong antimicrobial activity. *Langmuir* 23, 8670–8673. doi: 10.1021/la701067r
- Lee, J. A., Halbert, S. E., Dawson, W. O., Robertson, C. J., Keesling, J. E., and Singer, B. H. (2015). Asymptomatic spread of huanglongbing and implications for disease control. *P Natl Acad Sci U S A* 112, 7605–7610. doi: 10.1073/pnas.1508253112
- Li, H. P., Zhou, B., Lin, Y., Gu, L. R., Wang, W. K., Fernando, S., et al. (2004). Selective interactions of porphyrins with semiconducting single-walled carbon nanotubes. *J. Am. Chem. Soc.* 126, 1014–1015. doi: 10.1021/ja037142o
- Liu, H. M., Xu, Z., Wang, N., Yu, C., Gao, N. Y., Zhao, J. W., et al. (2010). Theoretical investigation on the chemical sensing of metalloporphyrin-based molecular junction. *J. Chem. Phys.* 132:244702. doi: 10.1063/1.3456542
- Mammanna, A., Asakawa, T., Bitsch-Jensen, K., Wolfe, A., Chaturantabut, S., Otani, Y., et al. (2008). Synthesis and characterization of water-soluble free-base, zinc and copper porphyrin-oligonucleotide conjugates. *Bioorgan Med Chem.* 16, 6544–6551. doi: 10.1016/j.bmc.2008.05.041
- Martin, K. E., Tian, Y., Busani, T., Medforth, C. J., Franco, R., van Swol, F., et al. (2013). Charge effects on the structure and composition of porphyrin binary ionic solids: ZnTPPS/SnTMePyP nanomaterials. *Chem Mater.* 25, 441–447. doi: 10.1021/cm303595s
- Mehmoed, T., Liland, K. H., Snipen, L., and Saebø, S. (2012). A review of variable selection methods in Partial Least Squares Regression. *Chemometr Intell Lab.* 118, 62–69. doi: 10.1016/j.chemolab.2012.07.010
- Peng, G., Wu, S., Ellis, J. E., Xu, X., Xu, G., Yu, C., et al. (2016). Single-walled carbon nanotubes templated CuO networks for gas sensing. *J. Mater. Chem. C* 4, 6575–6580. doi: 10.1039/C6TC01722C
- Penza, M., Rossi, R., Alvisi, M., Signore, M. A., Serra, E., Paolesse, R., et al. (2010). Metalloporphyrins-modified carbon nanotubes networked films-based chemical sensors for enhanced gas sensitivity. *Sensor Actuat B-Chem.* 144, 387–394. doi: 10.1016/j.snb.2008.12.060
- Rapala, J., Erkkö, K., Kukkonen, J., Sivonen, K., and Lahti, K. (2002). Detection of microcystins with protein phosphatase inhibition assay, high-performance liquid chromatography-UV detection and enzyme-linked immunosorbent assay - comparison of methods. *Anal. Chim. Acta* 466, 213–231. doi: 10.1016/S0003-2670(02)00588-3
- Ryabenko, A. G., Dorofeeva, T. V., and Zvereva, G. I. (2004). UV-VIS-NIR spectroscopy study of sensitivity of single-wall carbon nanotubes to chemical processing and Van-der-Waals SWNT/SWNT interaction. Verification of the SWNT content measurements by absorption spectroscopy. *Carbon* 42, 1523–1535. doi: 10.1016/j.carbon.2004.02.005
- Sagaram, U. S., DeAngelis, K. M., Trivedi, P., Andersen, G. L., Lu, S. E., and Wang, N. (2009). Bacterial diversity analysis of huanglongbing pathogen-infected citrus, using phylochip arrays and 16S rRNA gene clone library sequencing. *Appl Environ Microb.* 75, 1566–1574. doi: 10.1128/AEM.02404-08
- Salvetat, J. P. G., Briggs, A. D., Bonard, J. M., Bacsá, R. R., Kulik, A. J., Stockli, T., et al. (1999). Elastic and shear moduli of single-walled carbon nanotube ropes. *Phys. Rev. Lett.* 82, 944–947. doi: 10.1103/PhysRevLett.82.944
- Sankaran, S., Ehsani, R., and Etxeberria, E. (2010). Mid-infrared spectroscopy for detection of huanglongbing (greening) in citrus leaves. *Talanta* 83, 574–581. doi: 10.1016/j.talanta.2010.10.008
- Sankaran, S., Mishra, A., Maja, J. M., and Ehsani, R. (2011). Visible-near infrared spectroscopy for detection of Huanglongbing in citrus orchards. *Comput. Electron. Agric.* 77, 127–134. doi: 10.1016/j.compag.2011.03.004
- Shirakawa, M., Fujita, N., and Shinkai, S. (2005). A stable single piece of unimolecularly pi-stacked porphyrin aggregate in a thixotropic low molecular weight gel: a one-dimensional molecular template for polydiacetylene wiring up to several tens of micrometers in length. *J. Am. Chem. Soc.* 127, 4164–4165. doi: 10.1021/ja042869d
- Shirsat, M. D., Sarkar, T., Kakoullis, J., Myung, N. V., Konnanath, B., Spanias, A., Mulchandani, A. (2012). Porphyrin-functionalized single-walled carbon nanotube chemiresistive sensor arrays for VOCs. *J Phys Chem C* 116, 3845–3850. doi: 10.1021/jp210582t
- Song, F. F., Ma, P., Chen, C. L., Jia, J. N., Wang, Y. C., and Zhu, P. H. (2016). Room temperature NO₂ sensor based on highly ordered porphyrin nanotubes. *J Colloid Interf Sci.* 474, 51–57. doi: 10.1016/j.jcis.2016.04.012
- Stephano-Hornedo, J. L., Torres-Gutiérrez, O., Toledano-Magaña, Y., Gradilla-Martínez, I., Pestryakov, A., Sánchez-González, A., et al. (2020). Argovit™ silver nanoparticles to fight huanglongbing disease in Mexican limes (*Citrus Aurantifolia Swingle*). *RSC Adv.* 10, 6146–6155. doi: 10.1039/C9RA09018E
- Wang, B., Zuo, X., Wu, Y. Q., Chen, Z. M., He, C. Y., and Duan, W. B. (2011). Comparative gas sensing in copper porphyrin and copper phthalocyanine spin-coating films. *Sensor Actuat B-Chem.* 152, 191–195. doi: 10.1016/j.snb.2010.12.006

- Xie, H., Li, Y. T., Lei, Y. M., Liu, Y. L., Xiao, M. M., Gao, C., et al. (2016). Real-time monitoring of nitric oxide at single-cell level with porphyrin-functionalized graphene field-effect transistor biosensor. *Anal. Chem.* 88, 11115–11122. doi: 10.1021/acs.analchem.6b03208
- Zahou, I., Hassen, L. B., Mlika, R., Ben Chaabane, R., Nasri, H., and Ben Ouada, H. (2016). Synthesis and investigation on optical and electrical properties of a triflate iron porphyrin: application as an optical BPA sensor. *Synthetic Met.* 221, 75–85. doi: 10.1016/j.synthmet.2016.07.020
- Zhao, Y. L., and Stoddart, J. F. (2009). Noncovalent functionalization of single-walled carbon nanotubes. *Accounts Chem Res.* 42, 1161–1171. doi: 10.1021/ar900056z

Conflict of Interest: The authors declare that the research was conducted in the absence of any commercial or financial relationships that could be construed as a potential conflict of interest.

Copyright © 2020 Wang, Ramnani, Pham, Villarreal, Yu, Liu and Mulchandani. This is an open-access article distributed under the terms of the Creative Commons Attribution License (CC BY). The use, distribution or reproduction in other forums is permitted, provided the original author(s) and the copyright owner(s) are credited and that the original publication in this journal is cited, in accordance with accepted academic practice. No use, distribution or reproduction is permitted which does not comply with these terms.